A Symmetrical Transformerless Hybrid Converter with Leakage Current Suppression

Tang, Zhongting; Yang, Yongheng; Su, Mei; Han, Hua; Blaabjerg, Frede

Published in:
Proceedings of 2019 IEEE Energy Conversion Congress and Exposition (ECCE)

DOI (link to publication from Publisher):
10.1109/ECCE.2019.8912748

Publication date:
2019

Document Version
Accepted author manuscript, peer reviewed version

A Symmetrical Transformerless Hybrid Converter with Leakage Current Suppression

Zhongting Tang[1], Yongheng Yang[2], Mei Su[1], Hua Han[1], and Frede Blaabjerg[2]
[1]School of Automation, Central South University, Changsha, China
[2]Department of Energy Technology, Aalborg University, Aalborg, Denmark
zta@et.aau.dk; yoy@et.aau.dk; sumeicsu@mail.csu.edu.cn; hua_han@126.com; fbl@et.aau.dk

***Abstract*—Considering the high efficiency and flexibility, the transformerless hybrid converters with multiple outputs attract more and more attention in residential PV applications. However, the leakage current issue should be addressed properly to meet certain stringent safety regulations and standards. In this context, this paper presents a new symmetrical transformerless hybrid converter with simultaneous AC and DC outputs, while at the same time suppressing the leakage current. More specifically, a symmetrical boost-filter inductor is employed in the proposed converter to maintain a constant common mode voltage. The corresponding modulation methods with leakage current suppression for this converter are also proposed. Additionally, the derivation of the hybrid converter is summarized and one of its family topologies is presented as an example. Simulations are performed on a 3-kW hybrid converter system. The results have validated the performance of the proposed converter in terms of strong leakage current suppression, high power quality and also flexible reactive power injection.**

Keywords—hybrid converter, transformerless, leakage current, multiple outputs, PV system.

I. INTRODUCTION

Photovoltaic (PV) power generation units are popular in modern residential power systems [1]-[3], but challenges are also associated due to its characteristics of intermittency and regional difference. In such applications, considering the versatility, converters with multiple outputs are employed to interface PV panels with AC and DC grids or loads [4]-[9]. In addition, with the high penetration of PV power generation systems, the requirements of low leakage current, flexible reactive power injection and high power quality are becoming mandatory in grid-friendly systems [1].

Generally, the hybrid converters with simultaneous DC and AC outputs can be divided into two types. One is the traditional two-stage PV inverters, where the separated power converts are cascaded or paralleled [4]. In the cascaded type, a DC-DC converter and an inverter (voltage source) are connected in series, and the voltage at the DC-link must be higher than the peak voltage of the AC output voltage. While in the paralleled type, one DC-DC converter is employed to generate the DC-bus voltage (also higher than the AC output peak voltage), and one converter is adopted for the DC output and another inverter is set for the AC output. Although it can have a wide range of input voltages, the power density is low due to the adoption of three converters. The other type is the stand-alone hybrid converter, which uses less power devices to achieve DC and AC outputs simultaneously [5], and in turn, leading to overall high power-density and low system cost. Additionally, the stand-alone hybrid converter has inherent shoot-through protection, which, to some extent, can alleviate the electromagnetic interference (EMI) and deadtime issues in the power converters [6]-[8]. For example, a family of hybrid converter topologies with one AC and one DC output were proposed in [5], where the control of the single-switch boost converter is replaced by a voltage-source inverter (VSI). Furthermore, in order to simultaneously provide *n* AC outputs and one DC output, hybrid multi-output converters in series and parallel modes were proposed in [9].

However, the above hybrid converters must address the leakage current issue in PV applications, as required in grid standards or regulations [10], [11]. The traditional method is to provide galvanic isolation using transformers, e.g., the high-frequency transformer in the DC-DC stage or the low-frequency transformer between the inverter and the AC grid. Obviously, the extra transformer increases the system volume and costs. To tackle this, transformerless hybrid converters with low leakage currents should be adopted for residential PV systems (i.e., low power level). For example, to achieve multiple outputs while maintaining a low leakage current, a transformerless hybrid converter was proposed in [12], where two extra power switches and one AC filter inductor are added in the VSI to clamp the common mode voltage (CMV) to zero in each operation mode. Although the leakage current can be successfully suppressed, the power density and inductance utilization are low. Moreover, the system cost is also relatively high.

Regarding the VSI, many transformerless topologies and modulation methods have been reported in the literature [14]-[17]. For instance, the conventional single-phase full bridge inverter (FBI) adopts the bipolar pulse width modulation (BP-PWM) to maintain a constant CMV [13]. Thus, a low leakage current. DC-decoupling-based inverters are proposed to decouple the DC-link and full-bridge inverter like in the H5 topology [14]. Another, the AC-decoupling-based inverters employ an AC-decoupling circuit to achieve isolation between the PV and the power grid, e.g., the AC-H6 topology [15] and the highly efficient and reliable inverter concept (HERIC) [16]. However, when comparing with hybrid converter in [12], the above transformerless inverters can only provide an AC output and have no inherent shoot-through protection capability. In addition, there is a lack of reactive power injection capability in these topologies, which is critical in grid-friendly and flexible PV systems and also defined in the IEEE Std 1547-2018 [11].

With the above concerns, this paper proposes a symmetrical transformerless hybrid converter, which is suitable for low power-level PV power generation systems. The proposed converter adopts symmetrical boost-filter inductors and takes an FBI topology as the controlled power stage. Similar to the stand-alone hybrid converter, the

This work was supported by the National Natural Science Foundation of China under Grant 51677195 and the Fundamental Research Funds in the Central South University under Grant 2019zzts277.

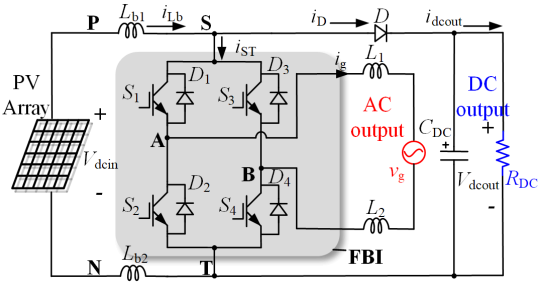

Fig. 1. Proposed transformerless hybrid converter with an (full-bridge inverter) FBI as the VSI.

proposed converter has the advantage of an inherent shoot-through protection. With its corresponding modulation scheme, this hybrid converter can also achieve DC and AC outputs simultaneously, low leakage current, high power quality and flexible reactive power injection, while the overall system cost is low.

The rest of this paper is organized as follows. Section II introduces the proposed symmetrical transformerless hybrid converter, its modulation strategy and also an CMV analysis. Then, the steady-state analysis of the proposed converter is presented in Section III, followed by the derivation methodology of the hybrid converter, where a topology from the derived family is exemplified. To verify the discussions, Section IV provides the simulation results. Finally, Section V gives the concluding remarks.

II. Proposed Symmetrical Transformerless Hybrid Converters

A. Symmetrical transformerless hybrid converter

As shown in Fig. 1, the symmetrical transformerless hybrid converter contains: (1) two symmetrical boost inductors, i.e., L_{b1} and L_{b2} with $L_{b1} = L_{b2}$, placed on the positive DC-link and negative DC-link rails, respectively; (2) a transformerless FBI topology, which is composed of the power devices S_1, S_2, S_3 and S_4 (with antiparallel diodes D_1, D_2, D_3 and D_4); (3) a power diode D and an output capacitor C_{DC} which are the basic components when acting as a DC-DC converter (for the DC output); (4) a symmetrical L-filter inductor ($L_1 = L_2 = L/2$), which is employed to ensure a good quality of the grid current.

Furthermore, in Fig. 1, P and N are the positive and negative terminal of the DC input V_{dcin}, S and T are the positive and negative terminal of the VSI input. In addition, v_g is the grid voltage, and V_{dcout} is the DC output voltage. The critical parameters include i_{Lb}, i_{ST}, i_D, i_{dcout} and i_g, which are the current of the symmetrical boost inductors, the VSI input current, the power diode current, the DC load current, and the grid current. The positive direction of the grid current i_g is defined as the current flowing from the VSI to the AC grid.

B. Modulation scheme

Fig. 2 shows the modulation scheme and key waveforms of the hybrid converter with the FBI as the VSI (Fig. 1), where P_V represents the positive output voltage mode, N_V represents the negative output voltage mode and ST is the shoot-through mode. When taking as a single-switch boost DC-DC converter, there are two intervals, i.e., one is the rising period for i_{Lb} during the shoot-through, and the other is the falling period for i_{Lb} in both the positive output voltage interval and negative output voltage interval. Furthermore, when considering the FBI, three voltage levels can be

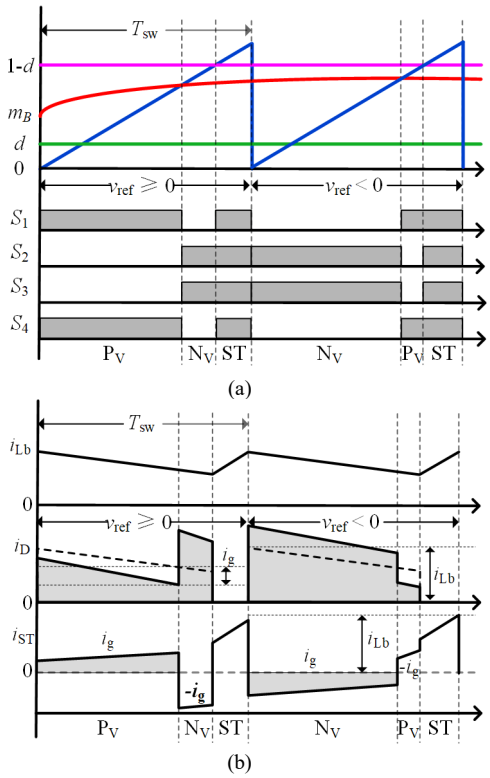

Fig. 2. Modulation scheme of the transformerless symmetrical hybrid converter with the FBI as the VSI (Fig. 1): (a) PWM signals and (b) key current waveforms, where T_{sw} is the switching period and v_{ref} is the ideal fundamental-frequency component of the differential mode voltage.

generated, i.e., zero voltage at the shoot-through mode, $+V_{dcout}$ at the positive output voltage mode and $-V_{dcout}$ at the negative output voltage mode.

The modulation scheme for the hybrid converter with the FBI as the VSI adopts a triangular wave carrier. As shown in Fig. 2(a), 1-d is the DC conversion ratio and m_B represents the modulation index of the FBI[18]. When the reference voltage $v_{ref} \geq 0$, i.e., the ideal fundamental-frequency component of the differential mode voltage (DMV), the interval for P_V is m_B and the interval for N_V is $1 - d - m_B$. While $v_{ref} < 0$, the N_V-interval is m_B and the P_V-interval is $1 - d - m_B$. Three key current waveforms are presented in Fig. 2(b), i.e., i_{Lb} is the boost filter current, i_D is the diode current and i_{ST} is the VSI input current.

C. Operation principle and CMV analysis

Assuming that the output filter inductances are identical, i.e., $L_1 = L_2$, the DMV V_{DM} (i.e., the output voltage of the FBI topology) almost has no effect on the leakage current. As it is shown in Fig. 1, the CMV V_{CM} and the DMV V_{DM} of the proposed hybrid converter structure can be defined as

$$V_{CM} = \frac{V_{AN} + V_{BN}}{2} \tag{1}$$

$$V_{DM} = V_{AT} - V_{BT} \tag{2}$$

where V_{AN} and V_{BN} are the voltages of terminals A and B to terminal N, and V_{AT} and V_{BT} are the voltages of terminals A and B to terminal T.

To simplify the analysis and better understand the operation modes, only the continuous conduction mode is considered in the hybrid converter when operating as a single-switch boost converter. It means that the inductor current is always larger than zero. The three operation modes,

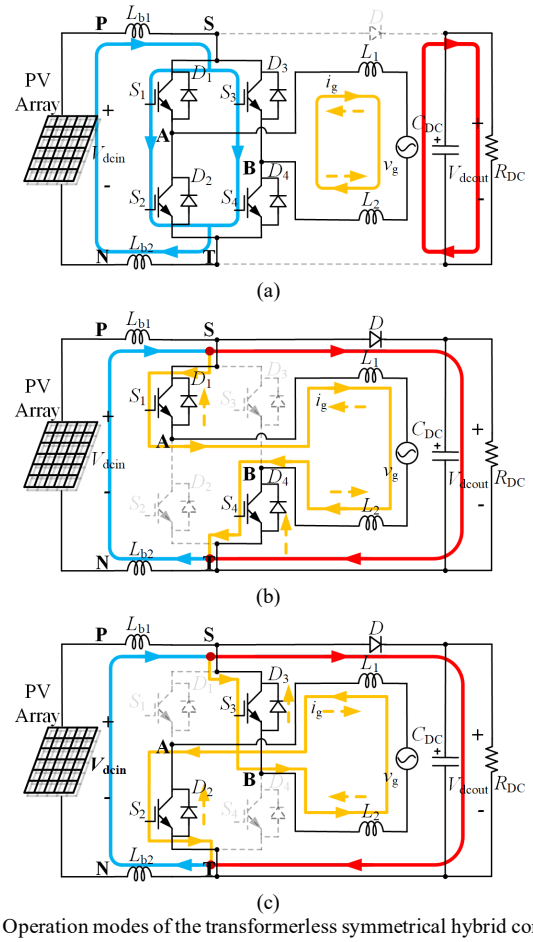

Fig. 3. Operation modes of the transformerless symmetrical hybrid converter with the FBI as the VSI: (a) shoot-through mode, (b) positive V_{DM} mode, and (c) negative V_{DM} mode, where V_{DM} is the differential-mode voltage.

i.e., the shoot-through mode, the positive V_{DM} mode and the negative V_{DM} mode, the corresponding analysis of the CMV and the DMV are detailed in the following according to the systems shown in Fig. 3.

1) *Shoot-through mode*: Fig. 3(a) illustrates the shoot-through mode. The FBI is taken as a boost switch, and all power devices (i.e., $S_{1\text{-}4}$) are in the ON-state. As shown in the *ST* interval in Fig. 2(b), L_{b1} and L_{b2} are charged by the PV array, and the boost inductor current i_{Lb} increases, and $V_{Lb1} = V_{Lb2} = V_{dcin}/2$. The power diode D is reverse-biased. The capacitor C_{DC} is discharged, supplying the DC load R_{DC}. In this operation mode, the CMV is clamped by the boost inductors L_{b1} and L_{b2}, and $V_{AN} = V_{BN} = V_{Lb2}$ and $V_{AT} = V_{BT} = 0$. Hence, the DMV V_{DM} and the CMV V_{CM} can be expressed as

$$V_{CM} = \frac{V_{AN} + V_{BN}}{2} = \frac{V_{Lb2} + V_{Lb2}}{2} = \frac{V_{dcin}}{2} \tag{3}$$

$$V_{DM} = V_{AT} - V_{BT} = 0 - 0 = 0 \tag{4}$$

Since $S_{1\text{-}4}$ are all in the ON-state, terminals A and B have been connected (i.e., $V_{AN} = V_{BN}$). Therefore, the grid current i_g just flows through the inductors L_1, L_2 and the grid v_g with a bidirectional path, as shown in Fig. 3(a). In this case, the FBI output voltage V_{DM} is equal to zero.

2) *Positive V_{DM} mode*: as shown in Fig. 3(b), the FBI operates as a VSI. The switches S_1 and S_4 are in ON-state while S_2 and S_3 are in OFF-state to achieve $V_{DM} = +V_{dcout}$. The boost current decreases and it simultaneously flows through the power diode and the FBI, as shown in Fig. 3(b) (i.e., the Pv-interval). The capacitor C_{DC} is charged, and the charging voltage is $V_{ST} = V_{dcout} = V_{dcin} + V_{Lb1} + V_{Lb2}$. In addition, V_{ST} also provides the load voltage. Since $V_{AN} = V_{dcin} + V_{Lb1}$, $V_{BN} = -V_{Lb2}$, $V_{AT} = V_{dcin} + V_{Lb1} + V_{Lb2}$ and $V_{BT} = 0$, V_{DM} and V_{CM} in Fig. 3(b) are calculated as

$$V_{CM} = \frac{V_{AN} + V_{BN}}{2} = \frac{V_{dcin} + V_{Lb1} + (-V_{Lb2})}{2} = \frac{V_{dcin}}{2} \tag{5}$$

$$V_{DM} = V_{AT} - V_{BT} = V_{dcin} + V_{Lb1} + V_{Lb2} - 0 = V_{dcout} \tag{6}$$

where the symmetrical boost filter voltages are equal, $V_{Lb1} = V_{Lb2}$. Regarding the FBI, there is also a bidirectional current path for the grid current i_g, i.e., $i_g \geqslant 0$, the grid current flows through S_1 and S_4 to achieve $V_{DM} = +V_{dcout}$; $i_g < 0$, the grid current flows through D_1 and D_4 to obtain $V_{DM} = +V_{dcout}$.

3) *Negative V_{DM} mode*: the FBI also works as a VSI, as presented in Fig. 3(c). S_2 and S_3 are in ON-state, while S_3 and S_4 are in OFF-state to achieve $V_{DM} = -V_{dcout}$. The boost filters are also in discharging mode and support the operation of the FBI, the charging of C_{DC} as well as the DC load, which is depicted as the *N*-interval in Fig. 2(b) and $V_{ST} = V_{dcout} = V_{dcin} + V_{Lb1} + V_{Lb2}$. In this mode, the terminal voltages are $V_{AN} = -V_{Lb2}$, $V_{BN} = V_{dcin} + V_{Lb1}$, $V_{AT} = 0$ and $V_{BT} = V_{dcin} + V_{Lb1} + V_{Lb2}$. Thus, V_{DM} and V_{CM} in Fig. 4(c) can be given as

$$V_{CM} = \frac{V_{AN} + V_{BN}}{2} = \frac{(-V_{Lb2}) + V_{dcin} + V_{Lb1}}{2} = \frac{V_{dcin}}{2} \tag{7}$$

$$V_{DM} = V_{AT} - V_{BT} = 0 - (V_{dcin} + V_{Lb1} + V_{Lb2}) = -V_{dcout} \tag{8}$$

in which the boost filter voltages are the same, $V_{Lb1} = V_{Lb2}$. Moreover, the FBI can also provide a bidirectional current path, i.e., $i_g \geqslant 0$, the grid current flows through D_2 and D_3 to let $V_{DM} = -V_{dcout}$; the grid current can flow through S_2 and S_3 to generate $V_{DM} = -V_{dcout}$.).

Owing to the inherent shoot-through protection, it is not necessary for the proposed hybrid converter to consider the deadtime effect in the modulation method. Seen from this perspective, compared with the traditional VSI [14]-[17], the proposed hybrid converter can result in a better performance in the overall reliability.

III. Steady- State Analysis

A. DC and AC conversion ratio

When taken as a single-switch boost converter [18], the relationship between the DC input voltage V_{dcin} and the DC output voltage V_{dcout} can be expressed as

$$V_{dcout} = \frac{V_{dcin}}{1-d} \tag{9}$$

$$d = 1 - \frac{V_{dcin}}{V_{dcout}} \tag{10}$$

where the shoot-through interval is d, and the FBI outputs zero voltage at this time. There is only $(1-d)T_{sw}$ time for the FBI to finish the inversion operation. It means that the FBI operation is constrained by

$$d + m_B \leq 1 \tag{11}$$

Therefore, the modulation index of the FBI m_B in steady-state can be calculated as

$$\left| \frac{v_g}{V_{dcout}} \right| = 2m_B - (1-d) \tag{12}$$

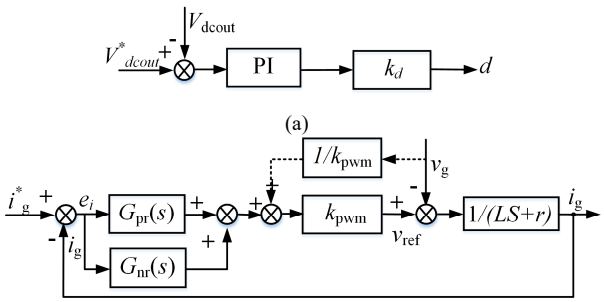

Fig. 4. Control diagram for the proposed hybrid transformerless converter with an FBI as the VSI. (a) Controller for DC output, and (b) Controller for AC output.

Substituting Eq. (9) into Eq. (11), and then m_B is obtained as

$$m_B = \frac{1}{2}(1-d)\left(1+\left|\frac{v_g}{V_{dcin}}\right|\right) \tag{13}$$

B. Control of the proposed hybrid converter

To simplify the control scheme, the PV input voltage V_{dcin} is assumed as a constant. The control system for the proposed symmetrical transformerless hybrid converter includes two parts, as shown in Fig. 4. The first one is a proportional integral (PI) controller employed in the voltage control-loop for the DC output. The other using a proportional-resonant (PR) controller $G_{pr}(s)$ in parallel with multi-resonant $G_{nr}(s)$ controllers is the current control loop, which has good performance in terms of the zero-error tracking and the background harmonic distortion elimination [19], [20]. In Fig. 4, k_d in the PI controller is the boost gain, and k_{pwm} is the inverter gain, which is equal to V_{dcout} in the proposed hybrid converter. In addition, only one resonant controller $G_{3r}(s)$ is adopted to simplify the parameters tuning process. In all, the good performance of dynamic response and power quality can also be achieved in this way.

C. Derivation methodology of hybrid converter

As shown in Fig. 5, the derivation method of the symmetrical transformerless hybrid converter can be summarized as: (1) two symmetrical boost inductors, i.e., L_{b1} and L_{b2} with $L_{b1} = L_{b2}$, should be placed on the positive DC and negative DC rails, respectively; (2) a transformerless VSI topology is adopted to clamp the CMV to the half of the DC input voltage with its corresponding modulation method; (3) a power diode D and a output capacitor C_{DC} are used for the DC-DC converter to supply DC loads; (4) a symmetrical output filter inductor network for a good current quality and also to decrease the impact from the DMV on the leakage current. Additionally, as shown in Fig. 5, Z_{GcGd} is the impedance between the PV parasitic capacitor C_{PVg} and ground, and i_{leak} is the leakage current.

According to the derivation methodology, another topology of the hybrid converters is presented in Fig. 6. This hybrid converter takes the HERIC inverter as the VSI, where S_1, S_2, S_3 and S_4 (with antiparallel diodes D_1, D_2, D_3 and D_4) form two basic inverter legs, and S_5 and S_6 (with antiparallel diodes D_5 and D_6) provide an AC bypass circuit to achieve the zero voltage during freewheeling. Correspondingly, the modulation method of this topology should be modified to achieve reactive power injection. Being different from the hybrid converter with the FBI as the VSI, there are four operation modes, i.e., the shoot-through mode, the positive V_{DM} mode, the negative V_{DM} mode, and the zero V_{DM} mode.

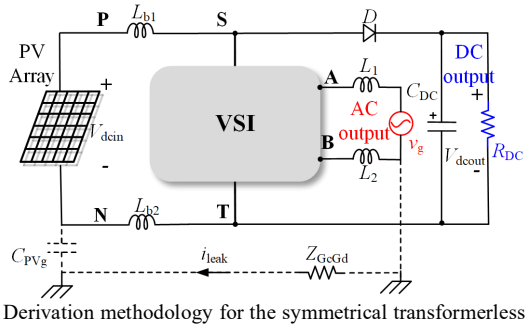

Fig. 5. Derivation methodology for the symmetrical transformerless hybrid converter.

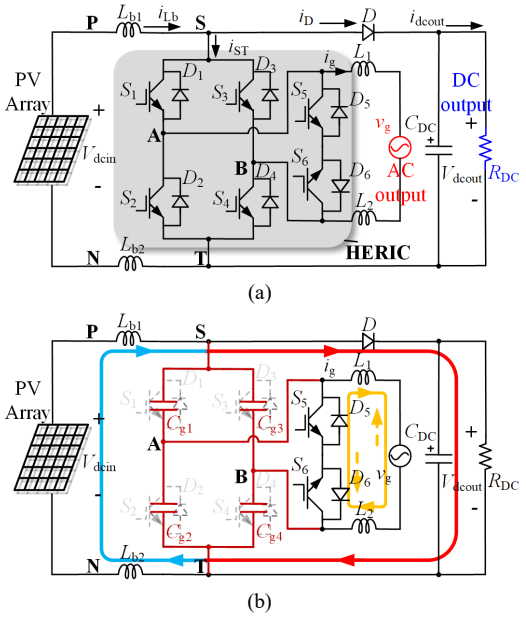

Fig. 6. An example of the symmetrical hybrid converter topologies with an HERIC as the VSI. (a) Topology and (b) Zero V_{DM} mode.

Except for the zero V_{DM} mode, the performance of the other three modes are the same as the hybrid converter with the FBI as the VSI. When at the zero V_{DM} mode, the CMV can be clamped to be $V_{dcin}/2$ by the parasitic capacitances $C_{g1\text{-}4}$ of the power devices $S_{1\text{-}4}$, as shown in Fig. 6(b). In addition, the modulation index m_U of the HERIC should be modified as

$$m_U = (1-d)\left|\frac{v_g}{V_{dcin}}\right| \tag{14}$$

Comparing the two proposed hybrid converters in Fig. 1 and Fig. 6(a), Controller the symmetrical transformerless hybrid converter with the FBI as the VSI has only four power switches, while the hybrid converter with the HERIC employs six power switches. However, the converter with the HERIC achieves higher efficiency and lower filter inductor requirement than that with the FBI due to the same performance with the adoption of the unipolar pulse width modulation (UP-PWM). However, both converters can ensure low leakage currents, simultaneously generate DC and AC outputs as well as achieve reactive power injection of the VSI.

IV. Simulation Results

The proposed symmetrical transformerless hybrid converter with the FBI as the VSI is validated through simulations on 3-kW converter systems, where the DC output power is 2 kW and the AC output power is 1 kW. The input voltage V_{dcin} for both is 200 V, and the output DC voltage is

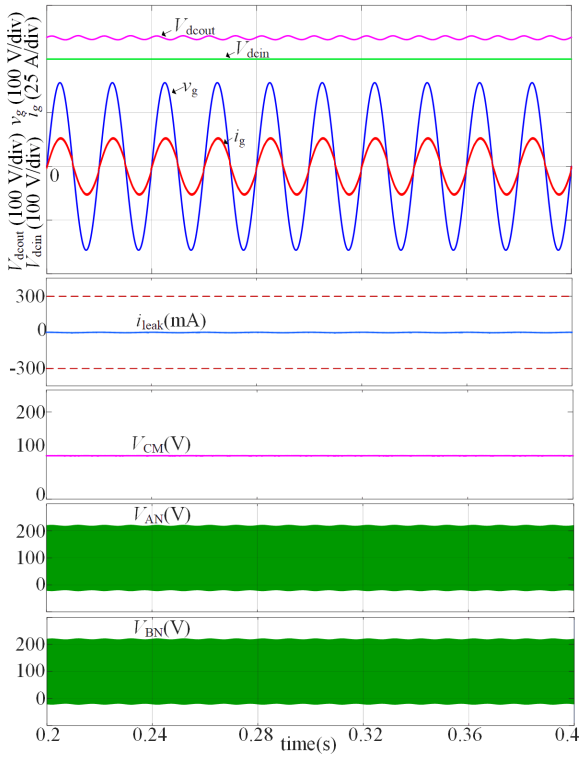

Fig. 7. Performance of the hybrid converter topology with the FBI as the VSI at unity power factor operation.

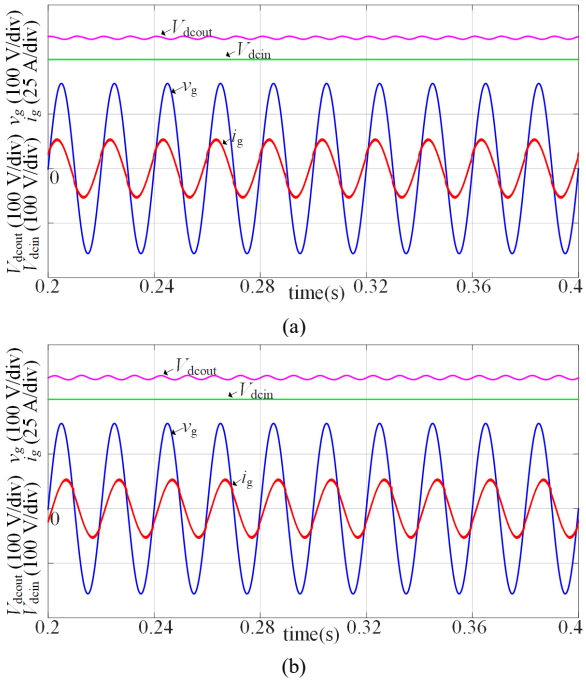

Fig. 8. Performance of the hybrid converter with the FBI as the VSI under non-unity power factors. (a) i_g leading v_g (cosφ = 0.8) and (b) i_g lagging v_g (cosφ = –0.8).

V_{dcout} = 240 V. The grid voltage is 110 V (root-mean-square) with the nominal frequency of 50 Hz. The boost inductor L_{b1} = L_{b2} = 0.75 mH and a capacitor C_{dc} = 2800 μF are adopted as the DC capacitor, and a DC resistive load R_{DC} = 30 Ω and the output inductor L_1 = L_2 = 1.5 mH are adopted. According to discussions in [21], the parasitic capacitance C_{PVg} of 300 nF is considered in the simulations.

Fig. 7 shows the simulation results of the hybrid converter with the FBI as the VSI, where V_{dcin}, V_{dcout}, v_g and i_g represent the DC input voltage, the DC output voltage, the grid voltage and the grid current, respectively. Additionally, i_{leak} is the leakage current, V_{CM} is the CMV voltage, and V_{AN} and V_{BN} are the voltages of terminals *A* and *B* to the terminal *N*. It can be observed that the hybrid converter can output DC and AC voltages, simultaneously. The DC voltage is 240 V as designed with the ripple voltage of 2.4 V (i.e., ±1% of V_{dcout}). The grid current is 9.09 A, as designed for the 1-kW AC output power. In addition, the CMV of the hybrid converter is almost a constant, i.e., V_{dcin}/2 = 100 V. Thus, the leakage current can be very lower than the limit in standards (i.e., 300 mA/RMS, the red dotted lines in Fig. 7). Furthermore, it can be seen from the performance of V_{AN} and V_{BN} that the DMV voltage of the hybrid converter changes between 0, +V_{dcout}, and -V_{dcout} at a high frequency.

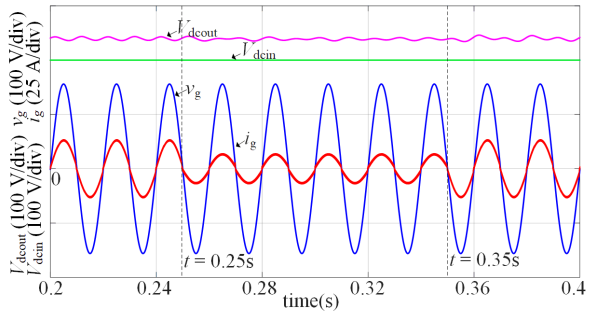

Fig. 9. Dynamic response of the hybrid converter with the FBI as the VSI, where the grid current i_g steps from 9.09 A to 4.54 A at t = 0.25 s, and steps from 4.54 A to 9.09 A at t = 0.35 s.

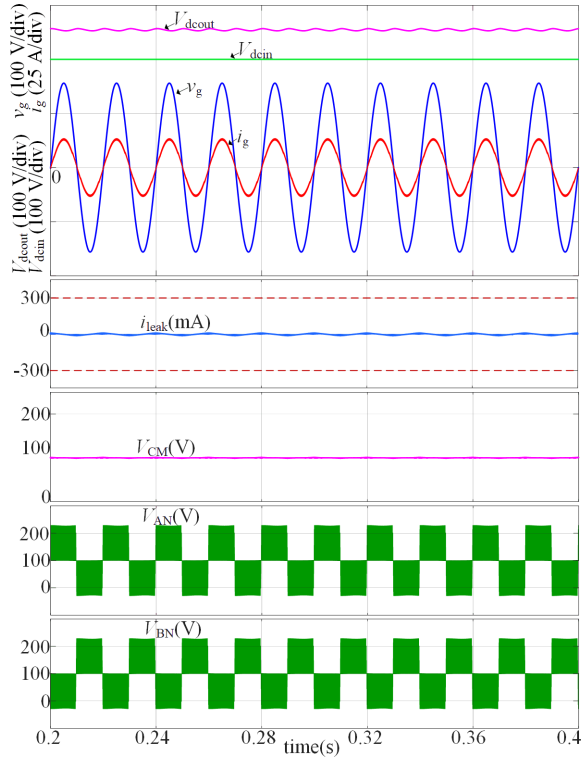

Fig. 10. Performance of the proposed hybrid converter topologies with the HERIC as the VSI (Fig. 5).

The performance of the hybrid converter with the FBI as the VSI under non-unity power factors (i.e., cosφ = ±0.8) is presented in Fig. 8. The power factor can be adjusted between +0.8 and –0.8 freely due to the proposed modulation scheme for the hybrid converter. Since the ST operation is a normal operation mode of the proposed converters, there is no dead time required during the operation. The power quality of the grid-connected current is higher than that of the conventional

VSI. The total harmonic distortion (THD) level of the hybrid converter with the FBI as the VSI is 4.57%, while the THD of the conventional FBI converter with the BP-PWM method is 5.53% at the same condition. Additionally, Fig. 9 shows the dynamic performance of the hybrid converter. The grid current i_g steps from 9.09 A to 4.54 A at $t = 0.25$ s, and steps from 4.54 A to 9.09 A at $t = 0.35$ s. The results illustrate that the hybrid converter has a good performance in terms of dynamic response.

To further validate the performance of the proposed converters, another simulation has been carried on a 3-kW hybrid converter with the HERIC as the VSI. The system parameters are the same as the hybrid converter with the FBI as the VSI. The results are shown in Fig. 10, where it can be observed that although the CMV will be affected slightly by the parasitic capacitance of the power devices of the converter, the leakage currents will also be very lower than the limit in the standards. Additionally, as shown in Fig. 10, the waveforms of V_{AN} and V_{BN} indicate that the DMV voltage of the hybrid converter with the HERIC as the VSI just changes between 0 and $+V_{dcout}/-V_{dcout}$. This means it operates with the UP-PWM. In addition, the THD of the grid current i_g in Fig. 10 is 2.43%. Therefore, the hybrid converter with the HERIC as the VSI has a better performance in terms of power quality and efficiency than that with the FBI.

In all, the simulations have confirmed that the proposed transformerless hybrid converter can simultaneously achieve AC and DC outputs with low leakage currents. The reactive power injection and good power quality can also be achieved. Thus, they can be promising candidates for PV systems.

V. Conclusions

This paper has proposed a symmetrical transformerless hybrid converter, which can simultaneously output DC and AC voltages. The proposed converter employs a symmetrical boost inductor to ensure a constant CMV and takes an FBI as the VSI for the inversion. The corresponding modulation method for the hybrid converter was also proposed to achieve the reactive power injection as well as low leakage currents. Moreover, the derivation method of the hybrid converter has been summarized and a representative hybrid topology with the HERIC as the VSI was presented, which has a higher efficiency and better power quality than the hybrid converter with the FBI as the VSI. However, in terms of the operation principle and leakage current suppression, the converter with the FBI is simpler with less power devices. Simulation results have validated that the proposed hybrid converter can achieve AC and DC outputs with low leakage currents and enable flexible reactive power injection. Additionally, many other transformerless topologies can be constructed according to the derivation methodology.

References

[1] Y. Yang, K. A. Kim, F. Blaabjerg, and A. Sangwongwanich, *Advances in Grid-Connected Photovoltaic Power Conversion Systems*, Woodhead Publisher/Elsevier, Aug. 2018. ISBN: 9780081023396.

[2] J. He and Y. W. Li, "Analysis, design, and implementation of virtual impedance for power electronics interfaced distributed generation," *IEEE Trans. Ind. Appl.*, vol. 47, no. 6, pp. 2525–2538, Nov./Dec. 2011.

[3] F. Blaabjerg, Z. Chen, and S. B. Kjaer, "Power electronics as efficient interface in dispersed power generation systems," *IEEE Trans. Power Electron.*, vol. 19, no. 5, pp. 1184–1194, Sept. 2004.

[4] R. Adda, O. Ray, S. K. Mishra, and A. Joshi, "Synchronous-reference-frame-based control of switched boost inverter for standalone DC nanogrid applications," *IEEE Trans. Power Electron.*, vol. 28, no. 3, pp. 1219–1233, Mar. 2013.

[5] O. Ray and S. Mishra, "Boost-derived hybrid converter with simultaneous DC and AC outputs," *IEEE Trans. Ind. Appl.*, vol. 50, no. 2, pp. 1082-1093, Mar.-Apr. 2014.

[6] Z. Tang, M. Su, Y. Sun, B. Cheng, Y. Yang, F. Blaabjerg, and L. Wang, "Hybrid UP-PWM scheme for HERIC inverter to improve power quality and efficiency," *IEEE Trans. Power Electron.*, vol. 34, no. 5, pp. 4292-4303, May 2019.

[7] H. Wang, Z. Wu, Z. Tang, H. Han, Y. Yang and F. Blaabjerg, "An Improved Modulation Strategy for the Active Voltage Clamping HERIC Inverter," in *Proc. of the IEEE Applied Power Electronics Conference and Exposition (APEC)*, Anaheim, CA, USA, 2019, pp. 1938-1942.

[8] Z. Tang, Y. Yang, M. Su, T. Jiang, F. Blaabjerg, H. Dan and X. Liang, "Modulation for the AVC-HERIC Inverter to Compensate for Deadtime and Minimum Pulse Width Limitation Distortions," in *IEEE Trans. Power Electron.*, pp. 1-1, Jun. 2019, Early Access Article. doi: 10.1109/TPEL.2019.2925549

[9] A. Ahmad, V. K. Bussa, R. K. Singh, and R. Mahanty, "Quadratic boost derived hybrid multi-output converter," *IET Power Electron.*, vol. 10, no. 15, pp. 2042-2054, Dec. 2017.

[10] VDE-AR-N 4105, "Power Generation systems connected to the low-voltage distribution network-Technical minimum requirements for the connection to and parallel operation with low-voltage distribution networks," Verband der Elektrotechnik, Aug. 2011.

[11] IEEE Standard for Interconnecting and Interoperability of Distributed Resources with Associated Electric Power Systems Interfaces, *IEEE Standard 1547.2*, 2018.

[12] S. Dey, V. K. Bussa and R. K. Singh, "Transformerless Hybrid Converter With AC and DC Outputs and Reduced Leakage Current," *IEEE J. Emerg. Sel. Top. Power Electron.*, vol. 7, no. 2, pp. 1329-1341, June 2019.

[13] T. Wu, C. Kuo, and H. Hsieh, "Combined unipolar and bipolar PWM for current distortion improvement during power compensation," *IEEE Trans. Power Electron.*, vol. 29, no. 4, pp. 1702-1709, Apr. 2014.

[14] H. Schmidt, C. Siedle, and J. Ketterer, "Wechselrichter zum umwandeln einer elektrischen gleichspannung in einen wechselstrom oder einen wechselspannung," EP Patent EP 1 369 985 A2, May 15, 2003.

[15] W. Yu, J. J. Lai, H. Qian, and C. Hutchens, "High-efficiency MOSFET inverter with H6-type configuration for photovoltaic nonisolated AC-module applications," *IEEE Trans. Power Electron.*, vol. 26, no. 4, pp. 1253-1260, Apr. 2011.

[16] S. Heribert, S. Christoph, and K. Jurgen, "Inverter for transforming a DC voltage into an AC current or an AC voltage," Europe Patent 1 369 985 (A2), May 13, 2003.

[17] W. Li, Y. Gu, H. Luo, W. Cui, X. He, and C. Xia, "Topology review and derivation methodology of single-phase transformerless photovoltaic inverter for leakage current suppression," *IEEE Trans. Ind. Electron.*, vol. 62, no. 7, pp. 4537-4551, Jul. 2015.

[18] R. W. Erickson and D. Maksimovic, *Fundamentals of Power Electronics*, 2nd ed. Norwell, MA: Kluwer, pp. 22-27, 2001.

[19] A. Timbus, M. Liserre, R. Teodorescu, P. Rodriguez, and F. Blaabjerg, "Evaluation of current controllers for distributed power generation systems," *IEEE Trans. Power Electron.*, vol. 24, no. 3, pp. 654–664, Mar. 2009.

[20] Y. Yang, K. Zhou, H. Wang, and F. Blaabjerg, "Analysis and mitigation of dead time harmonics in the single-phase full-bridge PWM converters with repetitive controllers," *IEEE Trans. Ind. Appl.*, vol. 54, no. 5, pp. 5343-5354, Sept./Oct. 2018.

[21] R. Araneo, S. Lammens, M. Grossi, and S. Bertone, "EMC Issues in high power grid-connected photovoltaic plants," *IEEE Trans. Electromagn. Compat.*, vol. 51, no. 3, pp. 639–648, Aug. 2009.